Published in final edited form as:
Anal Chem. 2009 August 1; 81(15): 6489–6495. doi:10.1021/ac900892u.

Ultrafast Differential Ion Mobility Spectrometry at Extreme Electric Fields in Multichannel Microchips

Alexandre A. Shvartsburg[†], **Richard D. Smith**[†], **Ashley Wilks**[‡], **Andrew Koehl**[‡], **David Ruiz-Alonso**[‡], and **Billy Boyle**[‡]
Biological Sciences Division, Pacific Northwest National Laboratory, P.O. Box 999, Richland, Washington 99352, and Owlstone Ltd, 127 Cambridge Science Park, Cambridge CB4 0GD, United Kingdom

Abstract

The maximum electric field intensity (E) in field asymmetric waveform ion mobility spectrometry (FAIMS) analyses was doubled to $E > 60$ kV/cm. In earlier devices with >0.5 mm gaps, such strong fields cause electrical breakdown for nearly all gases at ambient pressure. As the Paschen curves are sublinear, thinner gaps permit higher E: here, we established 61 kV/cm in N_2 using microchips with 35 μm gaps. As FAIMS efficiency is exceptionally sensitive to E, such values can in theory accelerate analyses at equal resolution by over an order of magnitude. Here we demonstrate FAIMS filtering in ~20 μs or ~1% of the previously needed time, with a resolving power of about half that for "macroscopic" units but sufficing for many applications. Microscopic gaps enable concurrent ion processing in multiple (here, 47) channels, which greatly relaxes the charge capacity constraints of planar FAIMS designs. These chips were integrated with a β-radiation ion source and charge detector. The separation performance is in line with first-principles modeling that accounts for high-field and anisotropic ion diffusion. By extending FAIMS operation into the previously inaccessible field range, the present instrument advances the capabilities for research into ion transport and expands options for separation of hard-to-resolve species.

Ion mobility spectrometry (IMS) distinguishes ion species based on transport properties in an inert buffer gas. Conventional or drift tube (DT) IMS that separates ions based on absolute mobility has been used in defense and security applications in the field, such as detection of explosives and chemical warfare agents, since the 1980s.[1] More recently, IMS (combined with mass spectrometry, MS) became topical in structural chemistry and in complex biological and environmental analyses.[1–11] The mobility for any ion–gas pair is a function of the ratio of electric field intensity (E) to the gas number density (N), which can be expressed[2] as a relative deviation (α) from the zero-field mobility $K(0)$ and expanded in infinite series of even powers over E/N:

$$K(E/N)=K(0)[1+\alpha(E/N)]=K(0)[1+a_1(E/N)^2+a_2(E/N)^4+\ldots+a_n(E/N)^{2n}] \quad (1)$$

This fact is exploited in differential IMS or field asymmetric waveform IMS (FAIMS) to filter ions by the difference between K at two E/N values.[2,3] A time-dependent electric field $E(\tau)$ with alternating segments of high E and low E of opposite polarity (but null mean E) is set up in a gap between two electrodes, through which ions are pulled by gas flow.[2,3] Hypothetical

Correspondence to: Alexandre A. Shvartsburg.
[†]Pacific Northwest National Laboratory.
[‡]Owlstone Ltd.

species with α = 0 at any *E/N* would oscillate together, but real ions drift across the gap with velocity proportional to the difference between the α values in the two segments and are neutralized on an electrode. For any particular species, the drift can be offset by motion caused by a constant "compensation field" (E_C) superposed on the time-dependent field. Scanning E_C reveals the spectrum of species present.[2,3] The E_C values depend on the $E(\tau)$ amplitude (the "dispersion field", E_D), and analytes are more fully characterized by maps[2] of E_C versus E_D. Species with equilibrium E_C close to the imposed value may still pass FAIMS because of finite gap width, diffusion, and Coulomb repulsion, which jointly control the spectral peak widths and thus the FAIMS resolution.[2,12]

The FAIMS electrodes may be curved, creating an inhomogeneous electric field that causes ion focusing,[3,13] or planar with a homogeneous field and thus no focusing.[2,3,14] As a consequence, a planar FAIMS is superior to a curved one in terms of resolution and the intrinsic resolution/sensitivity balance, quantification accuracy, and duty cycle for broad analyses.[14] For those reasons, stand-alone FAIMS[15,16] and GC/FAIMS[17–19] instruments use planar FAIMS designs. (The need to convey ions from the atmospheric pressure in FAIMS to the MS vacuum makes cylindrical or spherical FAIMS with ion focusing more attractive for FAIMS/MS systems.)[3]

Analyses using FAIMS of any geometry have been relatively slow, requiring a minimum ion residence time of $t \sim 1$–200 ms at a given E_C and thus ~0.1–30 s for a full scan. This has limited the options for introducing FAIMS between condensed-phase separations such as liquid chromatography (LC) or capillary electrophoresis (CE) and MS, where one or (preferably) several FAIMS scans should generally be completed within the elution time of a single LC or CE feature. To achieve that in conjunction with regular LC,[4,9] scanning E_C had to be replaced by stepping, which has compressed the FAIMS cycle but dropped the resolution below that obtainable, thus reducing the benefit of the FAIMS stage. The best FAIMS specificity is provided by $\{E_C; E_D\}$ maps, but those take at least an order of magnitude longer time to collect than a single E_C scan and thus were not compatible with online LC/MS analyses.

Here we report the development of FAIMS "microchips" that filter ions in ~20 μs, ~100–10 000 times faster than previous devices. For high ion transmission, the chips feature multiple parallel gaps. The performance of new analyzers has been evaluated employing a β-radiation ion source. The key to accelerated separation was raising the dispersion field to >60 kV/cm or approximately two times the previous maximum E_D used in FAIMS. Hence, we first discuss the foundations of extreme-field FAIMS, including the relationship between E_D, separation speed, and resolution, the engineering limitations on E_D due to electrical breakdown of gas that can be vacated in microscopic gaps, and the physical limitations caused by field healing of ions.

FUNDAMENTALS OF EXTREME-FIELD FAIMS

A trivial way to cut the FAIMS separation time is to truncate the gap or to speed up the flow in it, but as with other separations in media such as CE and DT IMS, the resolving power (*R*) of FAIMS normally scales[20] as $t^{1/2}$. For planar FAIMS, the peak width (full width at half-maximum, fwhm) is[2,21]

$$w = \frac{4}{K}\sqrt{\frac{\overline{D}_{II}\ln 2}{t}} = \frac{4N}{K_0 N_0}\sqrt{\frac{\overline{D}_{II}\ln 2}{t}} \quad (2)$$

where K_0 is the reduced mobility, defined as K at standard gas number density N_0, and $\overline{D}_{II}$ is the mean longitudinal diffusion coefficient for an ion over the $E(\tau)$ period, τ_c. The quantity $\overline{D}_{II}$ characterizes the anisotropic diffusion at high fields and always exceeds the isotropic diffusion constant D, which broadens the peaks. Then,

$$R=E_C/w=\frac{E_C K_0 N_0}{4N}\sqrt{\frac{t}{\overline{D}_{II}\ln 2}} \tag{3}$$

The utility of FAIMS is already limited[2] by modest resolving power of existing devices (typically ~10–20); hence, accelerating the analysis at the expense of R according to eq 3 is hardly attractive. Rather, one desires to translate the whole $R(t)$ curve to obtain higher resolution in equal time (or same separation faster) by changing other variables in eq 3: E_C/N and/or $\overline{D}_{II}$.

The E_C/N quantity equals[2,21]

$$E_C/N=-\sum_{n=1}^{\infty}\kappa_n(E_D/N)^{2n+1} \tag{4}$$

with the coefficients κ_n set by the a_n values in eq 1 and odd moments of the $E(\tau)$ profile, $\langle F_{2n+1}\rangle$,

$$\langle F_{2n+1}\rangle=\frac{1}{t_c E_D^{2n+1}}\int_0^{t_c}E^{2+n+1}(\tau)\mathrm{d}t \tag{5}$$

Thus, E_C/N for a particular ion depends on the dispersion field and the $E(\tau)$ profile that can be optimized for the best FAIMS resolution.[22] For the first term in eq 4,

$$\kappa_1=-a_1\langle F_3\rangle \tag{6}$$

Thus, E_C/N scales as E_D/N cubed if eq 1 is truncated after the quadratic term and possibly stronger accounting for further terms.

Denoting the gas molecule mass M and the gas temperature T, the quantity $\overline{D}_{II}$ equals[2,12]

$$\overline{D}_{II}=D[1+\langle F_2\rangle F_{II}MK_0^2N_0^2(E_D/N)^2/(3kT)] \tag{7}$$

where k is the Boltzmann constant and F_{II} is a property of the ion–molecule potential. The correction to D by eq 7 reflects the high-field diffusion term that scales as (E_D/N).[2] However, the value of D (at a fixed ion charge q) is proportional to $1/N$ by the Einstein relationship:[23]

$$D=kTK/q=kTK_0N_0/(qN) \tag{8}$$

So, $\bar{D}_{II}$ depends on E_D and N not as E_D/N; whether E_D/N is varied by changing E_D or N matters.

At constant gas pressure, the $\bar{D}_{II}$ (E_D) function evolves from flat in the zero-field limit to quadratic at very high E_D/N. Then, by eq 3, the scaling of FAIMS resolving power varies from E_D^3 at low E_D/N to E_D^2 at extreme E_D/N. This is a steep dependence regardless, and raising E_D drastically improves FAIMS resolution at equal separation time.[2,24–27] It is a yet more powerful path to quicker analyses: by eq 3, the speed of equivalent separation is proportional to $E_C^2/\bar{D}_{II}$ and thus to the *fourth* to *sixth power* of E_D. For example, doubling E_D would accelerate analyses by a factor of ~ 15–60. At a fixed dispersion field, the scaling of $\bar{D}_{II}$ as a function of $1/N$ ranges from linear in the zero-field limit to cubic at extreme E_D/N, and the scaling of R varies from $1/N^{2.5}$ to $1/N^{1.5}$, respectively. Indeed, decreasing the gas pressure also improves the FAIMS resolution.[28] Here the speed of equivalent separation is proportional to the *third* to *fifth power* of $1/N$. This dependence is weaker than that on E_D: in the above example, doubling E_D/N would accelerate analyses by 2 times more when E_D is increased than when the pressure is dropped. Also, the dipole alignment of ions by the electric field is controlled by (mainly) E_D rather than E_D/N, and higher E_D normally allows stronger alignment that may have major analytical benefits,[29,30] while lower N disrupts the alignment by promoting the rotational heating of ions.[30]

The high-field diffusion also affects the dependence of FAIMS resolution on ion mobility. In the low-mobility limit, where $\bar{D}_{II} = D$ by eq 8, eq 2 condenses to

$$w = 4\sqrt{kT\ln 2/(qKt)} \tag{9}$$

Thus, the peak width decreases at higher mobility as $K^{-1/2}$. With increasing K, the contribution of high-field diffusion grows and eventually dominates. In the high-mobility limit, eq 2 reduces to

$$w = 4E_D\sqrt{\langle F_2\rangle F_{II} MK\ln 2/(3qt)} \tag{10}$$

Now the peak width increases at higher mobilities, scaling as $K^{1/2}$. Hence, at some intermediate K values, the FAIMS resolution should not significantly depend on mobility.

The E_D/N value in FAIMS is capped by the voltage for electrical breakdown between the electrodes (U_B) that depends on gN (where g is the gap width) according to the Paschen curve for the specific gas.[31] Those curves are sublinear; thus, the maximum E_D/N [equal to $U_B/(gN)$] always increases in narrower gaps and at lower gas pressure. With air or N_2 at atmospheric pressure, narrowing the gap from g = 2 to 2.5 mm in Ionalytics/Thermo Fisher systems[13,29] and the PNNL planar FAIMS design[14] to 0.5 mm in the Sionex units[28,32] has enabled increasing E_D from 25 to ~30 kV/cm or E_D/N from ~100 to ~120 Townsend (Td). Dropping the pressure in a 0.5 mm gap to 0.42 atm has allowed E_D/N to be raised to ~230 Td.[28] Even stronger fields can be established in narrower gaps or at lower pressure. As the Paschen curves minimize at some gN, a voltage under that minimum (~200 V for N_2) induces no breakdown.[31] Thus, an arbitrarily high E_D/N is theoretically feasible in a gap that is narrow enough for any given pressure.

Another limitation on E_D/N in FAIMS is the distortion (dissociation or isomerization) of ions consequent upon the field heating. An above-thermal average ion–molecule collision velocity due to rapid ion drift in strong fields means elevation of the ion translational (and therefore vibrational) temperature above the gas temperature:[2]

$$T_1=T+\Delta T=T+MK^2E^2/(3k)=T+M(K_0N_0)^2(E/N)^2/(3k) \quad (11)$$

The isomerization of protein ions in FAIMS is controlled by the maximum T_1 at waveform peaks[33,34] where $E = E_D$. The typical K_D value for ESI-derived protein ions in N_2 under ambient conditions is ~1 $cm^2/(Vs)$, which leads to $\Delta T > 50$ °C and, with a room-temperature gas, $T_1 >$ 70 °C that often causes extensive denaturation.[35] Small ions of high mobility are heated even more, with ΔT reaching[33] ~100–200 °C. With increasing E_D, all polyatomic ions will eventually dissociate, setting a physical limit on the dispersion field. However, as FAIMS spectra normally lack fragments of covalently bound species, there is room to raise E_D for most analytes.

Extending FAIMS to stronger fields would also allow the measurement of $K(E/N)$ curves in the previously inaccessible range. Besides adding to the fundamental knowledge about ion transport phenomena and the ion–molecule interactions underlying them, this capability would create more flexibility in devising FAIMS methods for hard-to-resolve species.

In summary, extending FAIMS operation to higher E/N has both fundamental and analytical motivations. Considering the advantages of a stronger field over the reduced gas pressure identified above, we have chosen to achieve the former via narrowing the FAIMS gap.

INSTRUMENT DEVELOPMENT

The FAIMS filtering occurs in a serpentine channel with g = 35 μm and 115 mm total span (for the cross section of S = 4 mm^2), with the length of L = 300 μm. The channel is etched through a silicon chip with a face of 3.25 × 2.5 mm, about 50% of which is open (Figure 1). As the U-turns in the channel take up a negligible fraction of its span, the gap may be viewed as a stack of 47 identical planar channels. The gap surfaces are made of high-conductivity silicon and are electrically connected via gold layer deposition on both faces. The chip is packaged and mounted onto a printed circuit board.

An asymmetric voltage applied across the gap is synthesized using an RF oscillator. The waveform profile with amplitudes for the two polarities in the ratio 2:1 (Figure 2) is close to the bisinusoidal employed in much previous FAIMS work.[2,12,22] The computed odd moments of this profile that control separation are $\langle F_3 \rangle = 0.108$ and $\langle F_5 \rangle = 0.105$ or close to $\langle F_3 \rangle = 1/9$ and $\langle F_5 \rangle = 0.113$ for the bisinusoidal waveform with a 2:1 harmonic ratio that is near-optimum for many ions[2,22] and was adopted in FAIMS systems by Ionalytics/Thermo Fisher. However, the present $\langle F_2 \rangle = 0.244$ is less than 0.278 for that profile and, by eqs 2 and 7, the diffusional broadening at high field is lower. The amplitude of ion oscillations in the $E(\tau)$ cycle equals[2]

$$\Delta d=K(0)E_D\tau_c\Delta_F \quad (12)$$

where Δ_F characterizes the waveform profile: Δ_F is 0.214 here versus 0.234 for the bisinusoidal.[2] The slower diffusion and smaller ion oscillations for the present waveform compared to the bisinusoidal improves the ion transmission through FAIMS when other factors are equal.

The amplitude in the high-field segment ("dispersion voltage") is variable up to 214 V that corresponds to E_D = 61 kV/cm or, at ambient conditions, E_D/N = 250 Td. This is still far below the electrical breakdown threshold, estimated (for N_2) at ~700 Td using the Paschen law. For good ion transmission through FAIMS, Δd by eq 12 must be well within the gap width. Hence, there is a minimum waveform frequency ($\eta = 1/\tau_c$) that depends on the mobility of the species

of interest. As the greatest $K(0)$ for ions in ambient air or N_2 is ~3 $cm^2/(Vs)$, analyzing all ions at any enabled E_D requires $\eta \gg 11$ MHz. We employed $\eta = 28.5$ MHz, which should work except for smaller ions at higher E_D values. Simulations below show that higher η would be beneficial, but this already is by far the greatest rf frequency ever used in IMS or MS. The compensation field is created by a compensation voltage (CV) produced by bias amplifiers and superposed on the waveform, with the range of ± 11 V. This means a range of ±3 kV/cm for E_C or ±13 Td for E_C/N, which suffices for all ions explored so far at any E_D.

Ions are carried through the chip by N_2 at room temperature and pressure. To prevent signal saturation at the detector, the sample gas is diluted 10–500 times (depending on the analyte concentration) by gas recirculated from the FAIMS exhaust after purification through a hydrocarbon and molecular sieve scrubber. The gas is filtered through a heated 15 μm steel mesh to remove particulates and pumped to the chip by a rotary vane pump (Rietschle Thomas G045). The gas properties are characterized immediately after the chip by sensors of temperature (Analog Devices AD22100), humidity (Honeywell HIH4000), and differential pressure across the chip (Invensys SCX05DN). The flow rate (Q) up to 3.2 L/min is determined by calibration versus the differential pressure as a function of temperature. The typical Q values are 2–3 L/min, amounting to an average flow velocity of $v_F = Q/S$ = 8–12 m/s and nominal residence time (L/v_F) of 24–36 μs. The flow velocity in a gap varies from zero at a solid boundary to the maximum at the median,[36] where it exceeds the average value by ~50%. As ions that pass FAIMS travel near the median, the mean t is[37] ~0.7 L/v_F or, typically, ~15–25 μs.

Filtered ions are detected using a charge collector, a gold-plated hexagonal grid of 8 mm size with 32% open area, positioned 2.2 mm after the chip and biased relative to it at −30 V (for cations) or +30 V (for anions). The ion current impacting on the grid is measured using a transimpedance amplifier and integrated over 212μs periods. The results are saved on a control PC and displayed on a screen using custom software as spectra at a particular E_D value or $\{E_C; E_D\}$ maps over a designated E_D range.

This FAIMS device can accept ions from various sources. Small molecules are commonly ionized by β-radiation from a radioactive source. Here, we use a Ni^{63} source (a cylindrical foil of 8 mm diameter and 10.5 mm length with activity of 555 MBq) 8 mm upstream of the chip. The sample may be delivered to the intake using a positive pressure or drawn by the built-in pump.

The ion flux through FAIMS (especially a planar one without ion focusing) is constrained by the space-charge capacity,[12] which can severely impair sensitivity. As Coulomb forces are proportional to the charge density squared, they are greatly attenuated by streaming ions into multiple channels (or a laterally wide folded one). Hence, a multichannel chip allows scaling of the FAIMS current capacity by the number of channels (here 47). A short separation time in the present chips reduces the space-charge effects further.

EXPERIMENTAL EVALUATION OF THE FAIMS CHIP

To characterize the new FAIMS device, we chose dimethyl methyl phosphonate (DMMP), an organophosporus compound with ions that resist fragmentation and charge exchange. As DMMP is a simulant of chemical warfare agents (CWA), its ions were studied by DT IMS[38,39] and FAIMS[28,40,41] using E_D/N up to ~220 Td in air at reduced pressure[28] (Figure 3a,b). The β-ionization of DMMP vapors in atmospheric air produces (for cations) the protonated monomer (I), proton-bound dimer (II), and ubiquitous “reactant ion peak” (RIP)[28,38] comprising protonated clusters of some one to four waters from ambient humidity (III). The present $\{E_C; E_D\}$ map (Figure 3c) resembles that obtained using[28] the SVAC device by Sionex

within the overlapping E_D/N range (Figure 3a), identifying all three traces. The assignment of the RIP is confirmed by the spectrum for the blank (Figure 3d). A slight difference between the shapes of traces I and II in panels a and c of Figure 3 at higher E_D/N may be due to different waveform profiles[22] and/or unequal air humidity. The detection limits (at signal/noise ratio of 4) were <0.1 ppb for DMMP, lower for compounds that are easier to ionize (e.g., ~0.02 ppb for dichlorophenol) and higher for others (e.g., aromatics).

In both FAIMS data sets, the features weaken and disappear as E_D increases in the order {III, II, I}, with a trace of I or its fragments continuing to maximum E_D (Figure 3a,c). This is consistent with predictions based on the dissociation energy and mobility of parent ions. That is, the standard enthalpy of formation ($\Delta H°$) for II (~130 kJ/mol)[39] is close to or exceeds that for III [decreasing from ~130 to ~50 kJ/mol as the clusters grow from one to four waters],[42] and the mobility of II [K_0 = 1.4 $cm^2/(Vs)$ in N_2 at room temperature] is smaller than that for III [2.1 $cm^2/(Vs)$].[38,39] Thus, water cluster ions are equally or less stable than DMMP dimers and are heated ~3 times stronger in a field. Hence, the feature III should vanish at lower E_D than II. The mobility[38,39] of I [K_0 = 1.8 $cm^2/(Vs)$] exceeds that of II, and DMMP monomers are always heated by ~60% more than the dimers. However, it is much harder to sever a covalent bond in the monomer than a hydrogen bond in the dimer, and I survive to higher E_D than II. In this chip (Figure 3c), all three species survive to higher E_D/N than in the SVAC (Figure 3a), e.g., ~150 Td versus ~125 Td for RIP. This may reflect a greater kinetic shift for dissociation during the much shorter time of present analyses.

The ion oscillation amplitude in an $E(\tau)$ cycle is proportional to E_D and the mobility of each species, hence raising E_D increases that amplitude and thus the ion loss in FAIMS. This would cause all features to disappear in the order of decreasing mobility {III, I, II}, while actually I survives to higher E_D than II (Figure 3a,c). Thus, this mechanism cannot fully explain the data with either FAIMS system but likely contributes to the decay as detailed below based on simulations.

The separation spaces in panels a and c of Figure 3 have nearly equal widths (~5 Td), as they should, given the similar E_D/N ranges for best resolution of all three species. The peaks I and II have w = 0.4–0.5 Td here (Figure 3d) versus 0.2 Td with the SVAC (Figure 3b). (The RIP that comprises diverse clusters is ~3 times broader and is disconnected from the instrumental resolution.) The present peak capacity is ~10–12 versus ~25 for the SVAC. However, as the separation is ~100 times faster here than in SVAC (t ~ 20 μs versus ~ 2 ms),[28] the peak capacity production rate[5,43] is >40 times greater. While the drop of resolution by ~2–2.5 times is significant, making the present chip unsuitable for some FAIMS applications, many species are still separable and the dramatic acceleration of filtering opens major new analytical options.

One can also look at anions. For DMMP, one finds only[28,41] the RIP as in the blank (Figure 3e,f), assigned to O_2^- and $O_2^-(H_2O)_n$ clusters. Many other substances, including nitro explosives such as dinitrotoluene (DNT), produce intense signals and are routinely detected by IMS in the negative-ion mode.[44,45] In previous experiments,[44,45] the DNT anion has behaved as a “type A” ion, which means that K increases at higher E/N and thus (with $E_D > 0$) one finds negative E_C that decreases at greater E_D. Those studies were limited to E_D/N under ~100 Td, at which point E_C/N was[44,45] −0.2 to −0.4 Td. The present data (Figure 4) match those results but reveal the mobility properties of the DNT anion at higher E/N where K starts decreasing and hence E_C/N begins to increase and turns positive (at E_D/N ~ 130 Td), reaching >2 Td before the signal vanishes at E_D/N ~200 Td. This trend reversal at some E_D/N is inevitable for type A ions, as at higher E/N the ion–molecule collisions become more energetic and eventually approach the hard-shell limit where the mobility of any ion decreases with rising field intensity.[2]

MODELING OF FAIMS PERFORMANCE

To understand the broad capabilities of the new FAIMS chip, we computed its resolving power and ion transmission efficiency (that controls sensitivity) for representative species using the established model[12,14,32] where ions filtered in the gap experience diffusion, including the high-field and anisotropic components. The space-charge effect, minor in multichannel chips as discussed above, was ignored. Each simulation involved 2×10^5 ions. This unusually large number, permitted by the short residence time and absence of Coulomb interactions, has reduced the statistical errors in calculations to negligible levels.

Unlike for curved geometries, in planar FAIMS, the peak width and sensitivity depend only on absolute K and not its field dependence.[2,20,21] Hence, for comparison with measurements, a peak simulated for fixed K (which leads to $E_C = 0$) can slide along the E_C axis to align with the actual peak. The widths of thus derived features for the DMMP monomer and dimer [assuming $t = 20\ \mu$s and K_0 of 1.8 and 1.4 cm^2/(Vs), respectively] match the experiment within 5% (Figure 3d).

This agreement gives credence to peak widths and transmission efficiencies calculated for other species and conditions (Figure 5). The transmission through FAIMS always drops at higher K, because of faster diffusion by eq 8 and effective narrowing of the gap per eq 12.[2,22] For the scan in Figure 3d, the computed transmission efficiencies are 44% for II, 23% for I, and 12% for III (Figure 5a). For singly charged ions, this means fair sensitivity up to $K \sim 2.4$ cm^2/(Vs) that (with N_2 gas) covers virtually all polyatomic ions, including all peptides, drugs and their metabolites, and signatures of explosives and CWA[46–49] With increasing K, the peak width decreases until transmission drops to ~50% [for $K < 1.4$ cm^2/(Vs)] and then stabilizes at ~0.5 Td. This is consistent with the leveling of $w(K)$ dependence predicted above based on eqs 9 and 10. At $K < 1$ cm^2/(Vs), the transmission approaches 100% but resolution is rapidly lost (Figure 5a). Analyses of such species require extending the separation by slowing the flow in the gap: by the scaling laws for planar FAIMS,[22] the transmission drops with increasing t exponentially while the resolving power grows as $t^{1/2}$.

The transmission of any species worsens at stronger dispersion fields, also because of faster diffusion due to intensified field heating by eq 7 and effective gap narrowing. At the present maximum E_D, singly charged ions with $K >$ ~1.4 cm^2/(Vs) are largely lost in FAIMS (Figure 5a), which (with N_2 gas) excludes important medium-size species such as some amino acids, explosives, and CWA.[46–48] Fortunately, high-mobility ions are small and tend to have pronounced $K(E/N)$ dependences[29] that allow FAIMS separation at less than maximum E_D/N, where transmission through the chip is satisfactory (Figure 3). This limitation (that likely contributes to the fading of features at higher E_D in Figure 3) can be lifted by accelerating the flow through the gap. The peak width depends on E_D mildly, amounting to 0.7 Td at maximum E_D and, unless at near-100% transmission, counterintuitively increases at higher E_D/N (Figure 5a). This happens because, with planar FAIMS in the diffusion-limited regime, the peaks do not depend on the gap width but broaden when the field heating accelerates diffusion by eqs 7 and 10. The resolution still improves at higher E_D/N because the expansion of the separation space (Figure 3) generally outweighs the peak broadening. As we have concluded from eq 10, at the highest K values, the peaks start broadening with increasing mobility (Figure 5a).

At a given mobility, the diffusion coefficient is proportional to the inverse ion charge state (z) by eqs 7 and 8. Hence, this chip can analyze multiply charged ions with mobility exceeding the caps for $z = 1$ species (Figure 5b). For example, for $z = 3$, the gap at maximum E_D is passable up to $K \sim 2.0$ cm^2/(Vs). With N_2 gas, this encompasses all tryptic peptide ions produced by ESI.[49] By slowing the diffusion, multiple charging narrows the peaks at equal mobility: from eqs 9 and 10, the effect at any field is proportional to $z^{1/2}$. Simulations bear this out (Figure

5b), for example, increasing z from 1 to 3 (at maximum E_D) for ions with $K = 1$ cm^2/(Vs) narrows the peaks from 0.7 to 0.5 Td. The peak widths also decrease at equal transmission efficiency, such as from 0.8 to 0.4 Td at 50% transmission. Again, all above simulations are for $t \sim 20\mu$s, and the resolution can be improved by lengthening the separation according to the scaling laws.[2,22]

CONCLUSIONS

The resolving power of FAIMS (R) is ideally proportional to the cube of peak field intensity E_D and the square root of ion residence time t. Thus, the separation speed at constant R scales as $\sim E_D^6$, and even a modestly stronger field dramatically accelerates analyses. Electric breakdown had previously limited E_D in FAIMS to ~25–30 kV/cm, but higher fields are possible in thinner gaps.

We have developed FAIMS microchips with multiple channels of 35μm width, or ~ 15–70 times narrower than in preceding FAIMS designs. Such gaps permit raising E_D by ~2–3 times to >60 kV/cm, which should accelerate analyses at equal resolution by ~50–500 times. The actual chips have lower resolving power than "macroscopic" FAIMS stages but filter ions in $t \sim 20\ \mu$s, or ~10^2–10^4 times quicker. In principle, this allows scanning the full E_C/N range (about −4 to 4 Td) without compromising the resolution in ~1 ms and obtaining an $\{E_C; E_D\}$ map in ~10 ms. The present resolution suffices for many applications while exceptional separation speed removes essentially all throughput limitations on FAIMS utilization (in particular, with respect to adding upstream stages as in LC/FAIMS/MS). The partition of ions into multiple channels greatly increases the current capacity of the present chip over that of single-gap planar devices. Swift separation in the chip minimizes losses, leading to high sensitivity with the detection limits of <0.1 ppb for many low molecular weight compounds.

The new chips were employed in a portable FAIMS unit with a β-radiation ion source and charge detection. The measured resolution is in excellent agreement with established scaling laws and a priori simulations of ion dynamics including anisotropic diffusion, showing the applicability of existing FAIMS theory to operation at extreme fields.

The tolerance of FAIMS chips to extreme fields allows extending the characterization of ion transport properties and ion–molecule potentials to a hitherto inaccessible region. Inter alia, the knowledge of $K(E/N)$ curves over a much broader E/N range permits fitting the a_n values in eq 1 for higher n, which are informative of the higher-order ion–molecule collision integrals[23] and are critical for evaluating the utility of higher-order differential IMS concepts.[2,50]

When the detector is not biased, most ions exiting the present chip are not captured. This allows the addition of subsequent stages such as MS or conventional IMS, while still monitoring the FAIMS spectra using the charge collector. The development and evaluation of a FAIMS/MS system based on the FAIMS microchip, including the analyses of multiply charged ions generated by ESI, will be reported separately.

Acknowledgments

Portions of this work were supported by the Battelle Independent R&D program, NIH NCRR, and PNNL LDRD-funded Initiative for Explosives Detection. We thank Drs. E. G. Nazarov and L Jamieson for their data on DMMP ions and Drs. K Tang and D. Toutoungi for insightful discussions.

References

1. Eiceman, GA.; Karpas, Z. Ion Mobility Spectrometry. CRC Press; Boca Raton, FL: 2004.

2. Shvartsburg, AA. Differential Ion Mobility Spectrometry: Nonlinear Ion Transport and Fundamentals of FAIMS. CRC Press; Boca Raton, FL: 2008.
3. Guevremont R. J Chromatogr, A 2004;1058:3. [PubMed: 15595648]
4. Venne K, Bonneil E, Eng K, Thibault P. Anal Chem 2005;77:2176. [PubMed: 15801752]
5. McLean JA, Ruotolo BT, Gillig KJ, Russell DH. Int J Mass Spectrom 2005;240:301.
6. Tang K, Li F, Shvartsburg AA, Strittmatter EF, Smith RD. Anal Chem 2005;77:6381. [PubMed: 16194103]
7. Valentine SJ, Plasencia MD, Liu X, Krishnan M, Naylor S, Udseth HR, Smith RD, Clemmer DE. J Proteome Res 2006;5:2977. [PubMed: 17081049]
8. Kolakowski BM, Mester Z. Analyst 2007;132:842. [PubMed: 17710259]
9. Canterbury JD, Yi XH, Hoopmann MR, MacCoss MJ. Anal Chem 2008;80:6888. [PubMed: 18693747]
10. Vakhrushev SY, Langridge J, Campuzano I, Hughes C, Peter-Katalinic J. Anal Chem 2008;80:2506. [PubMed: 18269265]
11. Thalassinos K, Grabenauer M, Slade SE, Hilton GR, Bowers MT, Scrivens JH. Anal Chem 2009;81:248. [PubMed: 19117454]
12. Shvartsburg AA, Tang K, Smith RD. J Am Soc Mass Spectrom 2004;15:1487. [PubMed: 15465362]
13. Barnett DA, Belford M, Dunyach JJ, Purves RW. J Am Soc Mass Spectrom 2007;18:1653. [PubMed: 17662612]
14. Shvartsburg AA, Li F, Tang K, Smith RD. Anal Chem 2006;78:3706. [PubMed: 16737227]
15. Miller RA, Eiceman GA, Nazarov EG, King AT. Sens Actuators, B 2000;67:300.
16. Eiceman GA, Krylov EV, Tadjikov B, Ewing RG, Nazarov EG, Miller RA. Analyst 2004;129:297. [PubMed: 15042159]
17. Eiceman GA, Tadjikov B, Krylov E, Nazarov EG, Miller RA, Westbrook J, Funk P. J Chromatogr, A 2001;917:205. [PubMed: 11403471]
18. Nazarov EG, Miller RA, Eiceman GA, Stone JA. Anal Chem 2006;78:4553. [PubMed: 16808465]
19. Kendler S, Lambertus GR, Dunietz BD, Coy SL, Nazarov EG, Miller RA, Sacks RD. Int J Mass Spectrom 2007;263:137.
20. Shvartsburg AA, Smith RD. J Am Soc Mass Spectrom 2007;18:1672. [PubMed: 17723907]
21. Krylov EV, Nazarov EG, Miller RA. Int J Mass Spectrom 2007;266:76.
22. Shvartsburg AA, Smith RD. J Am Soc Mass Spectrom 2008;19:1286. [PubMed: 18585054]
23. McDaniel, EW.; Mason, EA. Transport Properties of Ions in Gases. Wiley; New York: 1988.
24. Barnett DA, Guevremont R, Purves RW. Appl Spectrosc 1999;53:1367.
25. Barnett DA, Ells B, Guevremont R, Purves RW. J Am Soc Mass Spectrom 1999;12:1279.
26. Purves RW, Barnett DA, Ells B, Guevremont R. J Am Soc Mass Spectrom 2001;12:894. [PubMed: 11506222]
27. Cui M, Ding L, Mester Z. Anal Chem 2003;75:5847. [PubMed: 14588025]
28. Nazarov EG, Coy SL, Krylov EV, Miller RA, Eiceman GA. Anal Chem 2006;78:7697. [PubMed: 17105161]
29. Shvartsburg AA, Bryskiewicz T, Purves RW, Tang K, Guevremont R, Smith RD. J Phys Chem B 2006;110:21966. [PubMed: 17064166]
30. Shvartsburg AA, Noskov SY, Purves RW, Smith RD. Proc Natl Acad Set USA 2009;106:6495.
31. Meek, JM.; Craggs, JD. Electrical Breakdown of Gases. Wiley; New York: 1978.
32. Krylova N, Krylov E, Eiceman GA, Stone JA. J Phys Chem A 2003;107:3648. [PubMed: 12830828]
33. Shvartsburg AA, Li F, Tang K, Smith RD. Anal Chem 2007;79:1523. [PubMed: 17297950]
34. Robinson EW, Shvartsburg AA, Tang K, Smith RD. Anal Chem 2008;80:7508. [PubMed: 18729473]
35. Li J, Taraszka JA, Counterman AE, Clemmer DE. Int J Mass Spectrom 1999;185/186/187:37.
36. Schlichting, H. Boundary-Layer Theory. McGraw-Hill; New York: 1979.
37. Shvartsburg AA, Tang K, Smith RD. J Am Soc Mass Spectrom 2005;16:1447. [PubMed: 16006140]
38. Spangler GE, Vora KN, Carrico JP. J Phys E: Sci lnstrum 1986;19:191.
39. Ewing RG, Eiceman GA, Harden CS, Stone JA. Int J Mass Spectrom 2006;255–256:76.

40. Krylova N, Krylov E, Eiceman GA, Stone JA. J Phys Chem A 2003;107:3648. [PubMed: 12830828]
41. Krylov EV, Coy SL, Nazarov EG. Int J Mass Spectrom 2009;279:119.
42. Dalleska NF, Honma K, Armentrout PB. J Am Chem Soc 1993;115:12125.
43. Grall A, Leonard C, Sacks R. Anal Chem 2000;72:591. [PubMed: 10695147]
44. Buryakov IA. Talanta 2003;61:369. [PubMed: 18969196]
45. Eiceman GA, Krylov EV, Krylova NS, Nazarov EG, Miller RA. Anal Chem 2004;76:4937. [PubMed: 15373426]
46. Beegle LW, Kanik I, Matz L, Hill HH. Anal Chem 2001;73:3028. [PubMed: 11467550]
47. Kanu AB, Hill HH. Talanta 2007;73:692. [PubMed: 19073090]
48. Steiner WE, Clowers BH, Matz LM, Siems WF, Hill HH. Anal Chem 2002;74:4343. [PubMed: 12236341]
49. Baker ES, Clowers BH, Li F, Tang K, Tolmachev AV, Prior DC, Belov ME, Smith RD. J Am Soc Mass Spectrom 2007;18:1176. [PubMed: 17512752]
50. Shvartsburg AA, Mashkevich SV, Smith RD. J Phys Chem A 2006;110:2663. [PubMed: 16494377]

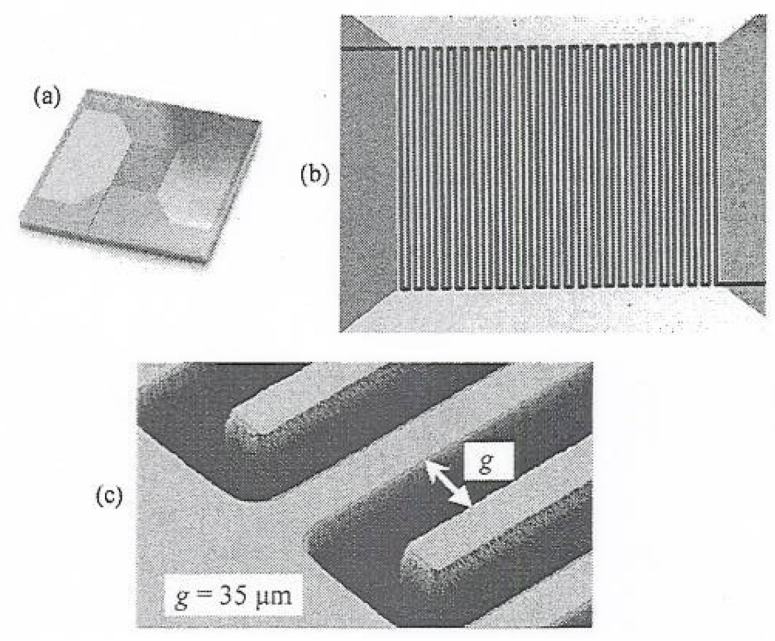

Figure 1.
Photo of the FAIMS microchip (a), its face exhibiting the serpentine channel (b), and electron micrograph showing detail of the gap entrance (c).

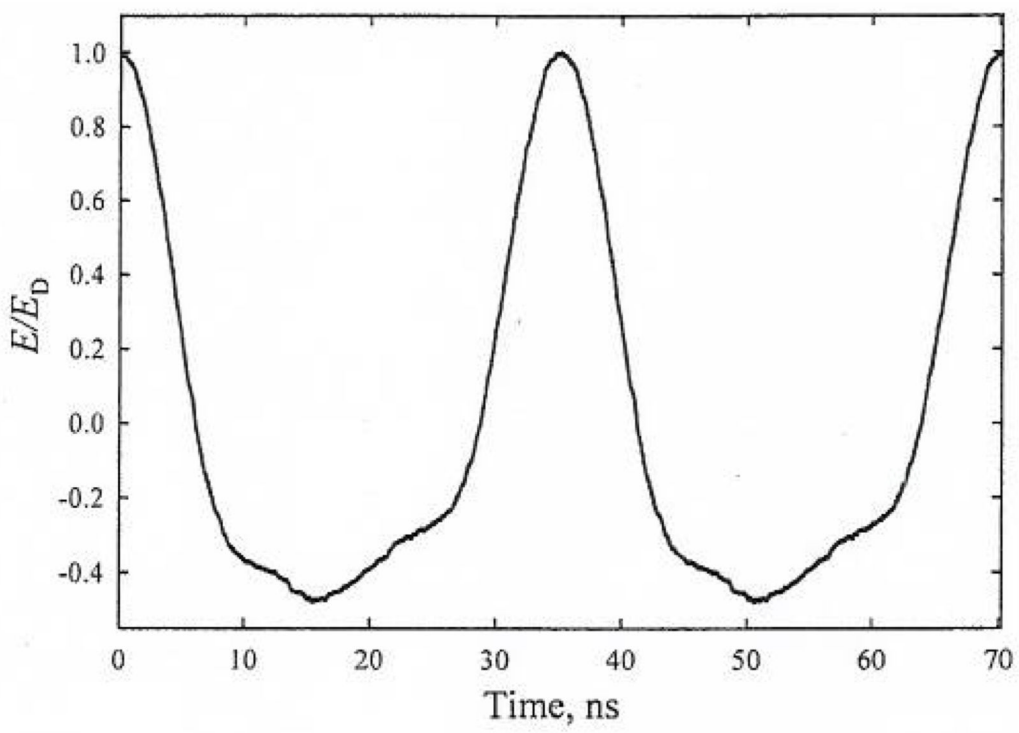

Figure 2.
Waveform profile used in the present FAIMS chip.

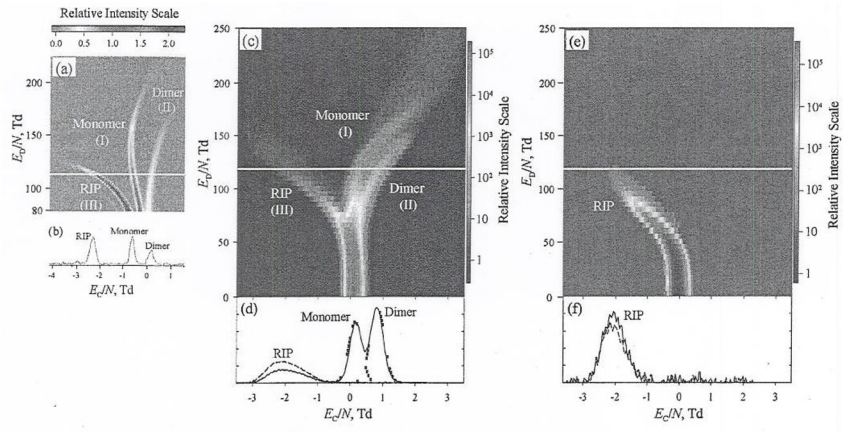

Figure 3.

FAIMS analyses of ions from the DMMP vapor at 4.6 ppm in air (a, b) and 0.59 ppb (upon dilution by 20 times) in N_2 (c–f). $\{E_C; E_D\}$ maps for cations obtained using the SVAC unit at 0.51 atm pressure (a) and the present system with Q = 2.5 L/min (c). The E_C scans at the E_D values marked by white bars (b, d). The present $\{E_C; E_D\}$ map and E_C scan for anions (e, f). The panels (d, f) show measurements for the sample (solid line) and the blank (dashed line), and (in d) simulations (dotted line). The panels (a, b) were provided by Dr. E. G. Nazarov.

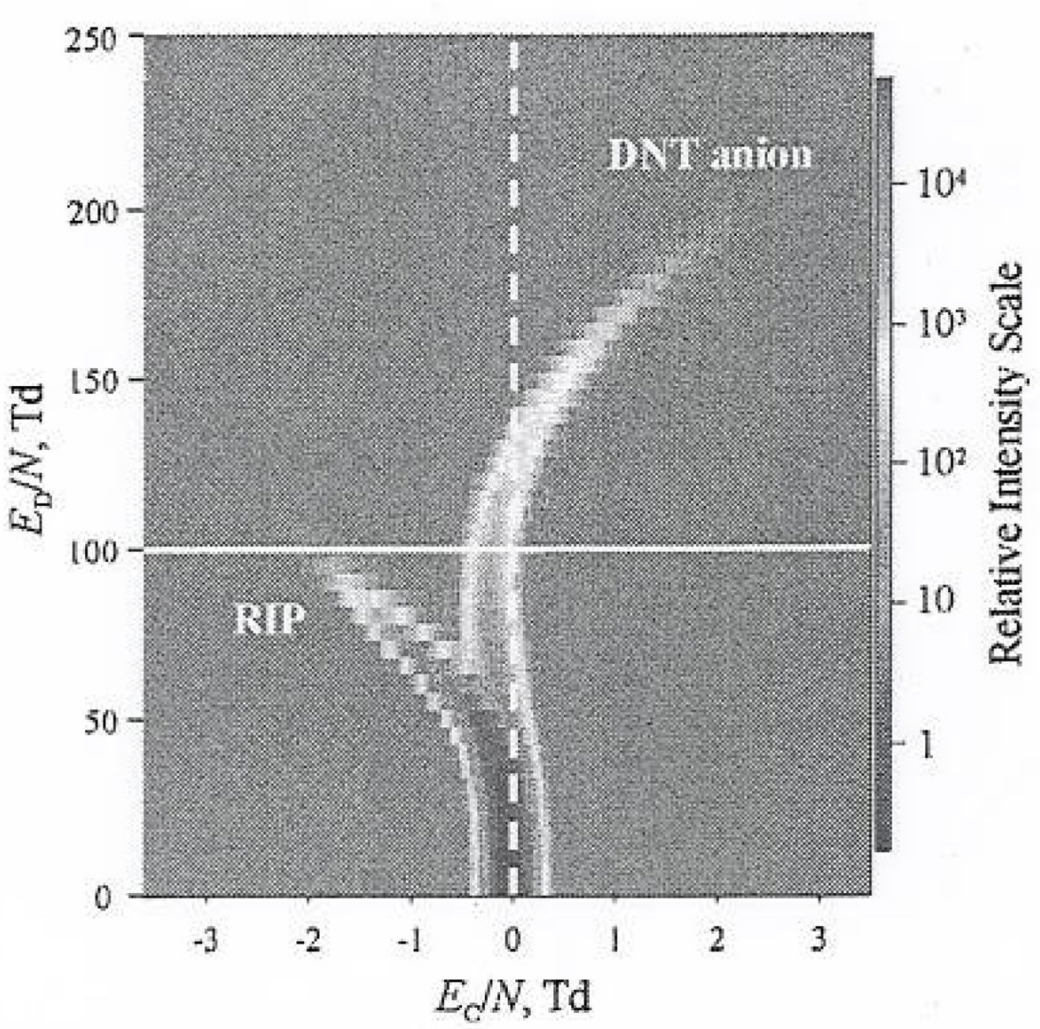

Figure 4.

{E_C; E_D} map for anions from the DNT vapor at 0.67 ppb (upon dilution by 20 times) in air, obtained at Q = 2.5 L/min. The horizontal white bar marks the upper E_D/N limit of previous measurements.[44,45]

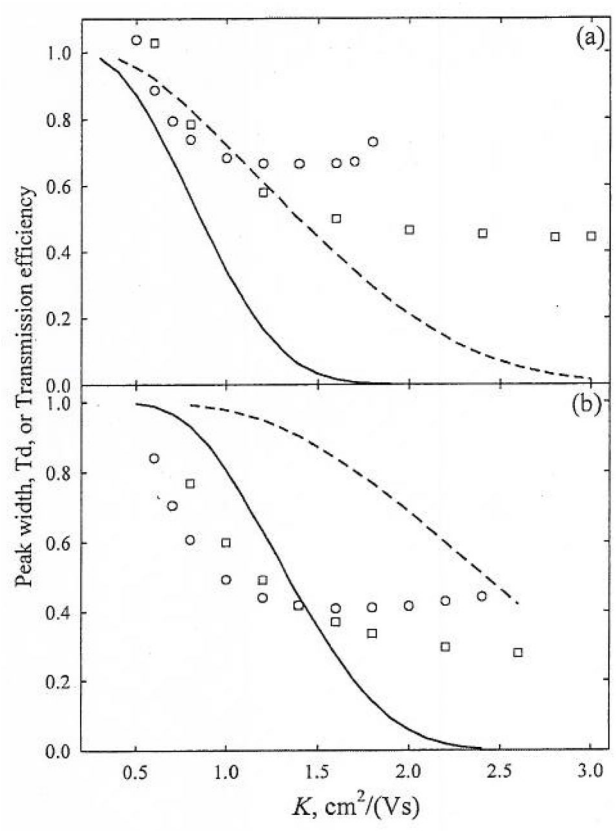

Figure 5.

Performance characteristics of the present FAIMS for species with $z = 1$ (a) and 3 (b) computed assuming $t = 20\ \mu s$: peak width (symbols) and transmission efficiency (lines). Circles and solid lines are for the maximum E_D/N of 250 Td; squares and dashed lines are for 120 Td.